FULL PAPER

Dalton
www.rsc.org/dalton

M···HNR interactions in imino-bound diaryltriazene complexes: structure and fluxionality

Christopher J. Adams, Kirsty M. Anderson, R. Angharad Baber, Neil G. Connelly, Mathivathani Kandiah and A. Guy Orpen
School of Chemistry, University of Bristol, Bristol, UK BS8 1TS.
E-mail: Neil.Connelly@bristol.ac.uk; Fax: +0117 929 0509; Tel: + 0117 928 8162

Received 3rd June 2004, Accepted 17th August 2004
First published as an Advance Article on the web 8th September 2004

The nominally square-planar coordination of the d^8 complexes [MClL^{1}L^2(*p*-XC$_6$H$_4$NNNHC$_6$H$_4$X-*p*)] (M = Rh, L^1 = L^2 = CO, X = H, Me, Et or F; M = Ir, L^1 = L^2 = CO, X = Me; M = Pd or Pt, L^1 = Cl, L^2 = PPh$_3$, X = Me; M = Pd, L^{1}L^2 = η^3-C$_3$H$_5$, X = Me), with the triazene *N*-bonded *via* the imine group, is supplemented by an axial M···H–N interaction involving the terminal amino group.

Introduction

Our previous studies of the synthesis of redox-active, triazenide-bridged binuclear complexes of Rh[1] and Ir[2] involved the deprotonation of metal triazene complexes preformed *in situ.* However, in order to synthesise analogous *hetero*bimetallic species[3] it proved advantageous to isolate the mononuclear triazene intermediates before use. We therefore give details of the synthesis and characterisation of square-planar triazene complexes of Rh, Ir, Pd and Pt, their structural characterisation, which has revealed an additional M···H–N axial interaction, and variable-temperature NMR spectroscopic studies which revealed a fluxional process involving interchange of the two aryl groups, R, of the triazene ligand RNNNHR.

Results and discussion

The complexes [RhCl(CO)$_2$(*p*-XC$_6$H$_4$NNNHC$_6$H$_4$X-*p*)] (X = H, **1**; Me, **2**; Et, **3**; F, **4**) (Table 1) were prepared by reacting [{Rh(μ-Cl)(CO)$_2$}$_2$] with the appropriate triazene in CH_2Cl_2. When the reaction was complete, as shown by IR spectroscopy (*ca.* 10 min), the solution was filtered, evaporated to low volume *in vacuo*, and then treated with *n*-hexane to give a yellow precipitate of the product. The iridium analogue of **2**, namely [IrCl(CO)$_2$(*p*-MeC$_6$H$_4$NNNHC$_6$H$_4$Me-*p*)] **5**, was prepared as before,[2] by reacting [{Ir(μ-Cl)(η^4-cod)}$_2$] (cod = cycloocta-1,5-diene) with *p*-MeC$_6$H$_4$NNNHC$_6$H$_4$Me-*p* in CH_2Cl_2 to give [IrCl(η^4-cod)(*p*-MeC$_6$H$_4$NNNHC$_6$H$_4$Me-*p*)] and then passing CO gas through the solution to displace cod.

The yellow complexes [PdCl(η^3-C$_3$H$_5$)(*p*-MeC$_6$H$_4$NNNHC$_6$H$_4$Me-*p*)] **6**, *trans*-[PtCl$_2$(PPh$_3$)(*p*-MeC$_6$H$_4$NNNHC$_6$H$_4$Me-*p*)] **7** and [PdCl$_2$(PPh$_3$)(*p*-MeC$_6$H$_4$NNNHC$_6$H$_4$Me-*p*)] **8** (the last as a mixture of *cis* and *trans* isomers) were prepared similarly by reacting *p*-MeC$_6$H$_4$NNNHC$_6$H$_4$Me-*p* with [{Pd(μ-Cl)(η^3-C$_3$H$_5$)$_2$}], [{Pt(μ-Cl)Cl(PPh$_3$)}$_2$] and [{Pd(μ-Cl)Cl(PPh$_3$)}$_2$], respectively.

Compounds **1–8** were characterised by elemental analysis, IR (Table 1) and NMR spectroscopy and, in the cases of **1**, **2**, **6** and **7**, by X-ray crystallography. The IR spectra of the carbonyl complexes **1–5** show two carbonyl bands in the region 2200–1900 cm^{-1} in agreement with the presence of a *cis*-M(CO)$_2$ group (M = Rh or Ir). There is little if any dependence of ν(CO) on the substituent X of the aryl group C$_6$H$_4$X-*p* but the iridium complex **5** shows carbonyl bands approximately 10–20 cm^{-1} lower in energy than those of the Rh complex **2**, in accord with the presence of the more electron rich iridium centre.

Each of the triazene complexes **1–8** shows a ν(NH) absorption in the range 3080–3110 cm^{-1} (Table 1), *cf.* the free triazene *p*-MeC$_6$H$_4$NNNHC$_6$H$_4$Me-*p* for which ν(NH) = 3199 cm^{-1}, indicating a weakening of the N–H bond even though the triazene ligand is bonded to the metal through the imine N atom (as shown by X-ray crystallography, see below).

The structures of 1, 2, 6 and 7

Crystals of **1**, **2**, **6** and **7** suitable for single crystal X-ray diffraction studies were obtained by allowing *n*-hexane to diffuse into a concentrated CH_2Cl_2 solution of the complex at −20 °C. The structures of **1**, **2**, **6** and **7** are shown in Figs. 1–4, respectively and selected structural data are given in Tables 2–4. Only the structure of **2** is discussed in detail, as a representative example, but differences from the structures of **1**, **6** and **7** are noted where appropriate.

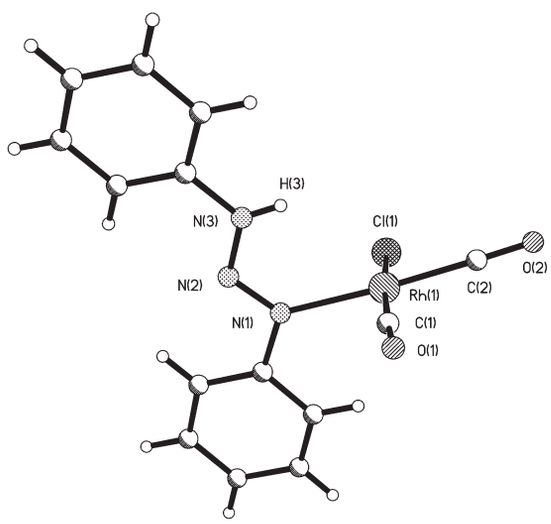

Fig. 1 The molecular structure of [RhCl(CO)$_2$(PhNNNHPh)] **1**.

The rhodium atom of **2** is bonded to two *cis* carbonyls, one chloride and the nitrogen atom of the imine, rather than the amine group, of the triazene ligand (Fig. 2). The metal is therefore effectively square planar. However, the triazene ligand is orientated in such a way as to bring the amine hydrogen atom H(3) close to the metal; the atoms Rh(1), N(1), N(2), N(3) and H(3) are coplanar and this plane is nearly perpendicular (at an angle of 81°) to the plane containing C(1), C(2), Cl(1) and N(1). Thus, H(3) is positioned above the metal, with a Rh(1)···H(3) distance of 2.647 Å (*cf.* 2.624 Å in **1**). This interaction between Rh(1) and H(3) results in a weakened N–H bond, and hence the energy of ν(NH) is lower than in the free triazene *p*-MeC$_6$H$_4$NNNHC$_6$H$_4$Me-*p*. The sole cause of the close proximity of the hydrogen atom and the metal appears to be the ligand geometry though the ligand is not especially distorted

DOI: 10.1039/b408410a

Table 1 Analytical and IR spectroscopic data for [MClL^{1}L^2(*p*-XC$_6$H$_4$NNNHC$_6$H$_4$X-*p*)]

					Analysis[a] (%)			IR/cm^{-1}	
	M	X	L^{1}L^2	Yield (%)	C	H	N	ν(CO)[b]	ν(NH)[c]
1	Rh	H	$(CO)_2$	60	43.6 (43.3)	2.8 (2.9)	10.7 (11.6)	2095, 2025	3086
2	Rh	Me	$(CO)_2$	81	45.8 (46.0)	3.6 (3.6)	10.0 (9.8)	2094, 2024	3109
3	Rh	Et	$(CO)_2$	78	48.3 (48.1)	9.4 (9.3)	4.3 (4.4)	2094, 2024	3108
4	Rh	F	$(CO)_2$	65	39.3 (39.4)	2.1 (1.7)	9.8 (9.5)	2096, 2026	3112
5	Ir	Me	$(CO)_2$					2083, 2005[d]	3078
6	Pd[e]	Me	$Cl(PPh_3)$	41	58.0 (58.0)	5.0 (5.0)	6.4 (6.2)		3097
7	Pd	Me	η^3-C_3H_5	83	49.9 (50.0)	4.9 (4.9)	10.4 (10.3)		3099
8	Pt	Me	$Cl(PPh_3)$	71	51.0 (51.1)	4.0 (3.7)	5.6 (5.6)		3091

[a] Calculated values in parentheses. [b] Strong absorptions in CH_2Cl_2. [c] Weak absorptions in Nujol. [d] Data from ref. 2. [e] Sample analysed as a 0.5 *n*-hexane solvate.

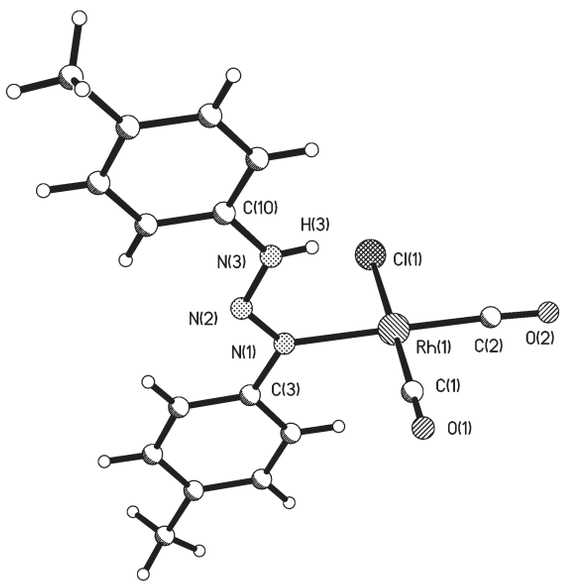

Fig. 2 The molecular structure of [RhCl(CO)$_2$(*p*-MeC$_6$H$_4$NNNHC$_6$H$_4$Me-*p*)] **2**.

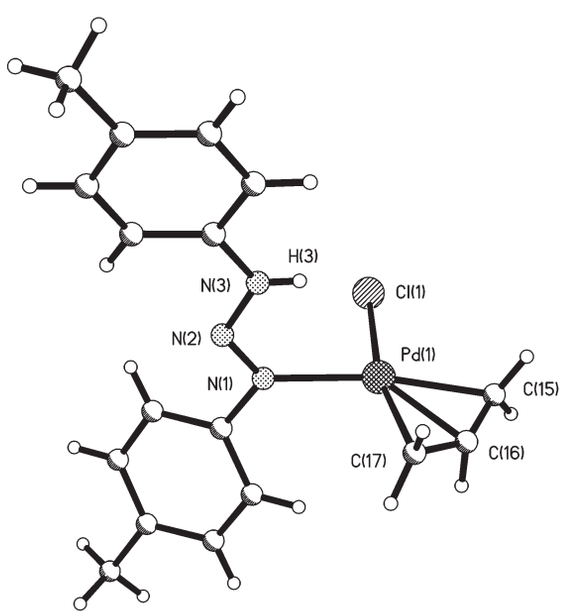

Fig. 3 The molecular structure of [PdCl(η^3-C$_3$H$_5$)(*p*-MeC$_6$H$_4$NNNHC$_6$H$_4$Me-*p*)] **6**.

to maximise the interaction. In fact, the angle M–N(1)–N(2) is greater than 120° in all four X-ray structures presented herein, which actually moves H(3) away slightly from the metal centre.

The coordinated triazene ligand in **2** has a *trans* conformation about both the N(1)–N(2) and N(2)–N(3) bonds; the sequence C(3)–N(1)–N(2)–N(3)–C(10) is almost planar with the N(1)–N(2)–N(3) angle 116°. The imine and amine tolyl groups are only slightly twisted with respect to this plane, by *ca.* 1 and 10°, respectively, bringing the *ortho* hydrogen atom of the imine tolyl ring into close proximity to the rhodium atom (2.651 Å). This interaction could be removed by twisting the tolyl group from the plane of the triazene unit, which does not occur in the solid state, but from the NMR spectroscopic data (see below) there is free rotation around this bond in solution. A similar situation is seen in the structure of **1**, with a hydrogen–metal distance of 2.662 Å.

Interestingly, for both **1** and **2**, the bond distances N(1)–N(2) and N(2)–N(3) are very similar to those of the free triazene PhNNNHPh[4] (Table 2). The former distance is shorter than the latter indicating that bond N(1)–N(2) has somewhat greater

Table 2 Selected bond lengths (Å) and angles (°) for RhCl(CO)$_2$(RNNNHR)] (R = Ph **1** or C$_6$H$_4$Me-*p* **2**)

	1	**2**	PhNNNHPh[a]
Rh(1)–C(1)	1.846(4)	1.889(4)	
Rh(1)–C(2)	1.854(3)	1.873(4)	
Rh(1)–Cl(1)	2.348(1)	2.358(1)	
Rh(1)–N(1)	2.097(2)	2.098(2)	
Rh(1)···H(3)	2.624	2.647	
C(1)–O(1)	1.127(4)	1.048(4)	
C(2)–O(2)	1.125(4)	1.123(4)	
N(3)–H(3)	0.783	0.775	
N(1)–N(2)	1.283(3)	1.277(3)	1.27
N(2)–N(3)	1.306(3)	1.311(3)	1.32
N(1)–Rh(1)–Cl(1)	89.9(6)	88.5(7)	
C(1)–Rh(1)–Cl(1)	175.9(1)	177.8(1)	
C(2)–Rh(1)–Cl(1)	87.3(1)	90.6(1)	
C(1)–Rh(1)–N(1)	92.4(1)	90.5(1)	
C(2)–Rh(1)–N(1)	176.5(1)	178.4(4)	
O(1)–C(1)–Rh(1)	177.4(3)	179.5(4)	
O(2)–C(2)–Rh(1)	177.8(3)	177.5(3)	
Rh(1)–N(1)–N(2)	125.4(2)	125.6(2)	
N(1)–N(2)–N(3)	116.2(2)	116.2(2)	115
N(3)–H(3)···Rh(1)	120.7	124.0	

[a] Data from ref. 4.

Table 3 Selected bond lengths (Å) and angles (°) for [PdCl(η^3-C$_3$H$_5$)(*p*-MeC$_6$H$_4$NNNHC$_6$H$_4$Me-*p*)] **6**

Pd(1)–Cl(1)	2.373(1)	C(15)–Pd(1)–Cl	98.9(2)
Pd(1)–C(15)	2.114(5)	C(16)–Pd(1)–Cl(1)	133.6(2)
Pd(1)–C(16)	2.056(6)	C(17)–Pd(1)–Cl(1)	167.5(2)
Pd(1)–C(17)	2.114(5)	C(16)–Pd(1)–C(15)	69.1(2)
Pd(1)···H(3)	2.718	C(17)–Pd(1)–C(15)	69.1(2)
Pd(1)–N(1)	2.102(4)	N(1)–Pd(1)–C(17)	99.7(2)
C(15)–C(16)	1.261(9)	N(1)–Pd(1)–C(15)	168.4(2)
C(16)–C(17)	1.257(10)	N(1)–N(2)–N(3)	116.3(3)
N(1)–N(2)	1.278(5)	C(15)–C(16)–C(17)	144.7(9)
N(2)–N(3)	1.305(5)	Pd(1)–N(1)–N(2)	127.8(3)
		N(3)–H(3)···Pd(1)	124.75

Table 4 Selected bond lengths (Å) and angles (°) for [$PtCl_2(PPh_3)$(*p*-$MeC_6H_4NNNHC_6H_4Me$-*p*)] **7**[a]

Pt(1)–Cl(1)	2.298(2)	2.310(2)	N(1)–Pt(1)–Cl(2)	86.30(14)	87.40(14)
Pt(1)–Cl(2)	2.293(2)	2.300(2)	N(1)–Pt(1)–Cl(1)	89.37(15)	87.69(14)
Pt(1)–P(1)	2.239(2)	2.250(2)	P(1)–Pt(1)–Cl(1)	89.00(7)	90.56(6)
Pt(1)···H(3)	2.598	2.680	P(1)–Pt(1)–Cl(2)	95.22(7)	94.44(6)
Pt(1)–N(1)	2.115(5)	2.107(5)	Cl(1)–Pt(1)–Cl(2)	173.56(8)	174.93(6)
N(1)–N(2)	1.259(7)	1.266(7)	N(1)–Pt(1)–P(1)	177.97(15)	175.09(16)
N(2)–N(3)	1.306(7)	1.305(8)	N(1)–N(2)–N(3)	117.0(5)	115.0(5)
N(3)–H(3)	0.87	0.80	Pt(1)–N(1)–N(2)	124.0(4)	128.3(4)
			N(3)–H(3)···Pt(1)	116.34	119.70

[a] There are two independent molecules in the asymmetric unit, and hence two possible values for each measurement.

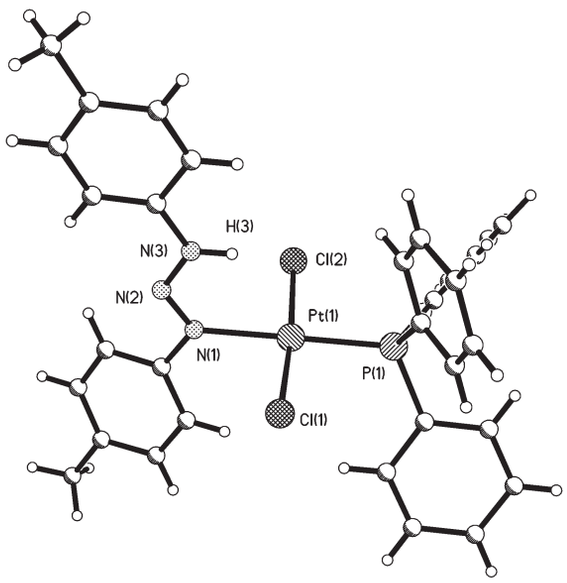

Fig. 4 The molecular structure of one of the independent molecules in the crystal structure of *trans*-[$PtCl_2(PPh_3)$(*p*-$MeC_6H_4NNNHC_6H_4$-Me-*p*)] **7**.

multiple bond character than N(2)–N(3). However, both distances lie between the values expected for an N=N double bond (*ca.* 1.12 Å) or an N–N single bond (1.37 Å), suggesting some delocalisation of π electrons along the N(1)–N(2)–N(3) fragment.

The molecular structure of [PdCl(η^3-C_3H_5)(*p*-MeC_6H_4NNN-HC_6H_4Me-*p*)] **6** (Fig. 3) is also approximately square planar with, for example, the angle N(1)–Pd(1)–Cl(1) = 92.5(1)° (Table 3). The C(15)–C(16)–C(17) angle of the allyl ligand is 144.7(9)°, with the central carbon atom C(16) effectively in the N(1)–Pd(1)–Cl(1) plane, and the two terminal atoms C(15) and C(17) on one side of this plane.

Unlike in complexes **1** and **2**, the triazene ligand *p*-$MeC_6H_4NNNHC_6H_4Me$-*p* is not planar; the amine tolyl and imine tolyl groups are twisted out of the N(1)–N(2)–N(3) plane by *ca.* 5 and 35°, respectively, and the torsion angle between the planes of the two tolyl groups is 21°. This has the effect of increasing the distance of the *ortho* proton of the imine tolyl group away from a site above the metal, unlike in **1** and **2**. As in **1** and **2**, however, the N(1)–N(2) and N(2)–N(3) bond lengths for **6** are in agreement with some delocalisation along the N(1)–N(2)–N(3) chain.

In crystals of **1**, **2** and **6** there are significant interactions between the Cl atom and both the N–H proton and an *ortho*-H atom on the amine tolyl ring from an adjacent molecule. These interactions lead to solid-state dimers, with similar intermolecular dimensions in all three cases (Table 5) and very similar motifs in the cases of **2** and **6** (Fig. 5).

The platinum atom of *trans*-[$PtCl_2(PPh_3)$(*p*-MeC_6H_4NNN-HC_6H_4Me-*p*)] **7** (Fig. 4, Table 4) is also approximately square planar, coordinated to one triazene, one PPh_3 and two *trans* Cl ligands; the asymmetric unit of the crystal structure contains two independent molecules with a very similar conformation.

Table 5 Intermolecular distances (Å) and angles (°) in the crystal structures of **1**, **2** and **6**

	1	**2**	**6**
CH···Cl	2.899	2.908	2.828
NH···Cl	2.629	2.629	2.780
C–H···Cl	129.85	144.79	146.89
N–H···Cl	148.93	153.19	153.83

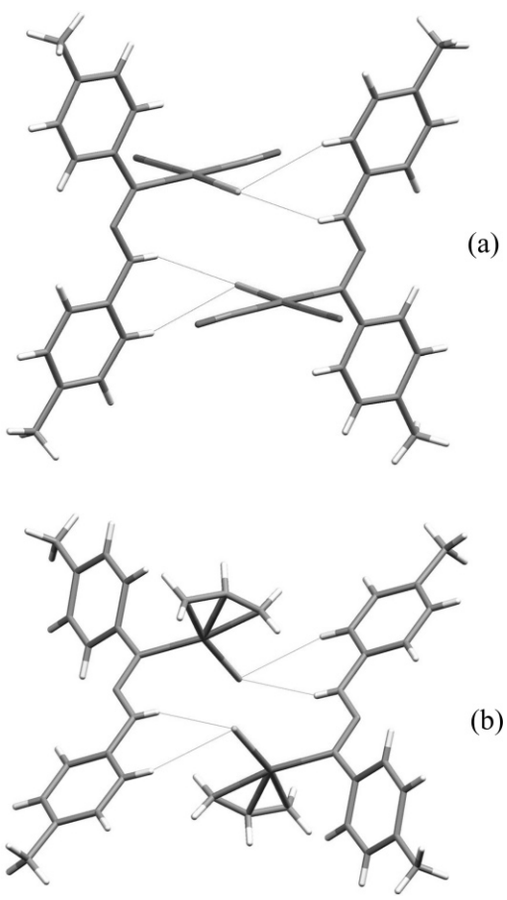

Fig. 5 Solid-state dimerisation of (a) **2** and (b) **6**.

The average values of the angles Cl(1)–Pt–Cl(2), N(1)–Pt–P(1), P(1)–Pt–Cl(2) and P–Pt–Cl(1) are 174.3(1), 176.5(2), 94.8(1) and 89.8(1)°, respectively. As in **1** and **2**, the Pt–N(1)–N(2)–N(3)–H(3) plane is almost perpendicular to the square plane about the metal, bringing the amine hydrogen atom H(3) in close contact with the metal [Pt···H(3), average value = 2.639 Å]. The structure of **7** shows no dimerisation of the kind shown by the structures of **1**, **2** and **6**; presumably the bulk of the PPh_3 ligand is sufficient to prevent the close approach of adjacent molecules.

The structure of **7** can also be compared with that of a closely related monodentate triazenide complex, namely square-planar *cis*-[$PtCl(PPh_3)_2$(*p*-$MeC_6H_4NNNHC_6H_4Me$-*p*)] **9** in which the

Table 6 ^{1}H and $^{13}C\{^{1}H\}$ NMR spectroscopic data for *trans*-[$PtCl_2$-(PPh_3)(*p*-$MeC_6H_4NNNHC_6H_4Me$-*p*)] **7** at 20 °C in CD_2Cl_2[a]

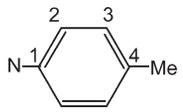

^{1}H	12.17 (s, 1H, NH), 8.12 (d, 2H, $^{1}J_{HH}$ 9, C_6H_4), 7.82–7.74 {m, 9H, $P(C_6H_5)_3$}, 7.58–7.45 {m, 6H, $P(C_6H_5)_3$}, 7.31 (d, 2H, $^{1}J_{HH}$ 9, C_6H_4), 7.29–7.24 (m, 4H, C_6H_4), 2.42 (s, 3H, CH_3), 2.38 (s, 3H, CH_3)
$^{13}C\{^{1}H\}$	145.70 (C^{1}), 139.04 (C^{1}), 135.92 (C^{4}), 135.82 (C^{4}), 134.02 (C^{3}, Ph), 133.88 (C^{3}, Ph), 131.70 (C^{2}), 129.95 (C^{2}), 128.62 (C^{2}, Ph), 128.47 (C^{2}, Ph), 127.60 (C^{4}, Ph), 126.75 (C^{4}, Ph), 122.06 (C^{3}), 115.97 (C^{3}), 21.43 (CH_3), 21.22 (CH_3)

[a] *J* values in Hz.

Pt–N(1), Pt–Cl and Pt–P (PPh_3 *trans* to Cl) bond lengths are 2.108(9), 2.353(7) and 2.11(2) Å, respectively,[5] similar to those of complex **7** (Table 4). However, while the N(1)–N(2) distance is similar for **7** and **9** [1.262(7) and 1.26(3) Å, respectively], the distance N(2)–N(3) [1.306(7) and 1.26(3) Å, respectively] is longer for the former, reflecting the difference between the amino and imino termini of the triazene and triazenide ligands, respectively. Moreover, the Pt–P distance *trans* to the nitrogen donor is shorter in **7** than in **9** [2.245(2) *cf.* 2.289(6) Å], perhaps indicating a stronger *trans* influence for the anionic triazenide ligand.

NMR spectroscopy

At temperatures between 20 and −80 °C, the ^{1}H NMR spectrum of [$PtCl_2(PPh_3)$(*p*-$MeC_6H_4NNNHC_6H_4Me$-*p*)] **7** is invariant, with resonances between 7.23 and 8.20 ppm for the aromatic protons of the diaryltriazene and PPh_3 ligands, two methyl resonances at δ 2.38 and 2.42 (Table 6), consistent with two different methyl environments, and one triazene NH proton signal at δ 12.17. Similarly, there are two methyl resonances in the $^{13}C\{^{1}H\}$ NMR spectrum, at δ 21.43 and 21.22. The $^{31}P\{^{1}H\}$ NMR spectrum shows a single resonance at δ 5.58, with platinum satellites, $J(^{195}Pt^{31}P)$ 3597 Hz. This, and the ^{1}H NMR spectrum therefore indicate the presence of only the *trans* isomer in solution (as shown by X-ray crystallography, see above).

By contrast, the ^{1}H NMR spectrum of **8**, the Pd analogue of **7**, shows *cis* and *trans* isomers in a 1 : 2 ratio (though it is not known which isomer is the more abundant). Thus, as well as several signals for the triazenide C_6H_4 protons between 6.9–8.0 ppm [Fig. 6(a)] there are four different Me singlets, in a 1 : 1 : 2 : 2 ratio, at δ 2.34, 2.28, 2.27 and 2.25 [Fig. 6(b)]. There are also two NH proton signals, at δ 11.63 and 11.45, and the $^{31}P\{^{1}H\}$ NMR spectrum shows two singlets, at δ 28.29 and 27.21, also in a 1 : 2 ratio.

Unlike for **7** and **8**, the variable temperature ^{1}H NMR spectra of complexes **1**–**4** and **6** show a fluxional process

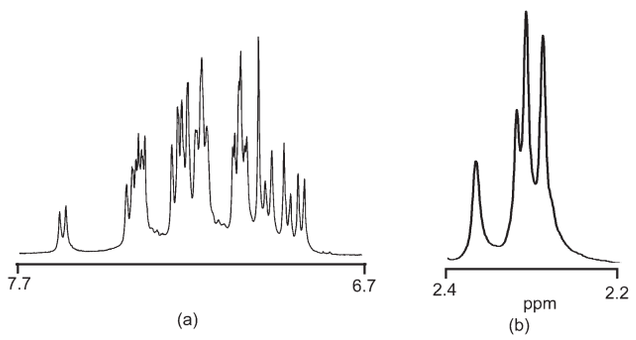

Fig. 6 ^{1}H NMR spectrum showing (a) the C_6H_4 and C_6H_5, and (b) the Me resonances of a mixture of *cis*- and *trans*-[$PdCl_2(PPh_3)$(*p*-$MeC_6H_4NNNHC_6H_4Me$-*p*)] **8**, at 20 °C.

Table 7 ^{1}H NMR spectroscopic data for [$MCl(CO)_2$(RNNNHR)] in CD_2Cl_2[a]

Complex	*T*/°C	Chemical shift/ppm
1	20	11.55 (s, 1H, NH), 7.90 (s br, 2H, C_6H_5), 7.46–7.35 (br, 6H, C_6H_5)
	−80	11.62 (s, 1H, NH), 7.95 (d, 2H, $^{1}J_{HH}$ 8, C_6H_5), 7.35 (m, 8H, C_6H_5)
2	20	11.50 (s, 1H, NH), 7.95 (s br, 2H, C_6H_4), 7.39–7.30 (br, 6H, C_6H_4), 2.39 (s, 6H, CH_3)
	−80	11.51 (s, 1H, NH), 7.81 (d, 2H, $^{1}J_{HH}$ 9, C_6H_4), 7.26 (d, 2H, $^{1}J_{HH}$ 9, C_6H_4), 7.22 (d, 2H, $^{1}J_{HH}$ 9, C_6H_4), 7.16 (d, 2H, $^{1}J_{HH}$ 9, C_6H_4), 2.34 (s, 3H, CH_3), 2.31 (s, 3H, CH_3)
3	20	11.44 (s, 1H, NH), 7.80 (s br, 2H, C_6H_4), 7.34–7.15 (br, 6H, C_6H_4), 2.60 (s, 4H, CH_2CH_3), 1.16 (s, 6H, CH_2CH_3)
	−80	11.53 (s, 1H, NH), 7.86 (d, 2H, $^{1}J_{HH}$ 8, C_6H_4), 7.28 (d, 2H, $^{1}J_{HH}$ 8, C_6H_4), 7.25 (d, 2H, $^{1}J_{HH}$ 9, C_6H_4),7.17 (d, 2H, $^{1}J_{HH}$ 8, C_6H_4), 2.61 (m, 4H, CH_3), 1.72 (m, 6H, CH_3)
4	20	11.50 (s, 1H, NH), 7.95 (s, br, 2H, C_6H_4), 7.39–7.30 (br, 6H, C_6H_4)
	−80	11.65 (s, 1H, NH), 7.96 (dd, 2H, $^{1}J_{HH}$ 8, $^{2}J_{HF}$ 5, C_6H_4), 7.36 (dd, 2H, $^{1}J_{HH}$ 8, $^{2}J_{HF}$ 5, C_6H_4), 7.15 (dd, 2H, $^{1}J_{HH}$ 8, $^{2}J_{HF}$ 8, C_6H_4), 7.06 (dd, 2H, $^{1}J_{HH}$ 8, $^{2}J_{HF}$ 8, C_6H_4)
5	20, −80	11.90 (s, 1H, NH), 7.89 (d, 2H, $^{1}J_{HH}$ 9, C_6H_4), 7.33 (d, 2H, $^{1}J_{HH}$ 9, C_6H_4), 7.30–7.21 (m, 4H, C_6H_4), 2.40 (s, 3H, CH_3), 2.38 (s, 3H, CH_3)

[a] Chemical shifts (δ) in ppm, *J* values in Hz.

involving exchange of the C_6H_4X-*p* groups of the triazene ligand. The ^{1}H NMR spectra of [$RhCl(CO)_2$(*p*-$XC_6H_4NNNHC_6H_4X$-*p*)] (X = H **1**, Me **2**, Et **3** and F **4**) (Table 7) show the C_6H_4 and NH protons of the triazene ligand between δ 6.50–7.50 and 11.40–11.90, respectively. At room temperature, [$RhCl(CO)_2$(*p*-$MeC_6H_4NNNHC_6H_4Me$-*p*)] **2** shows two broad peaks, at δ 7.80 and 7.37, one doublet at δ 7.27 for the C_6H_4 groups, and one singlet for the Me groups [Fig. 7(i)]. At −40 °C [Fig. 7(ii)], the two broad peaks and the methyl singlet are partially resolved into doublets, and at −80 °C [Fig. 7(iii)], two $(AB)_2$ splitting patterns are evident for the two C_6H_4 groups, centred at δ 7.48 and 7.24, with two Me resonances, at δ 2.31 and 2.34. Thus, the rate of exchange of the C_6H_4X-*p* groups is slowed at low temperature so that the amine and imine C_6H_4X-*p* groups are distinguishable.

The fluxional process which leads to equivalent C_6H_4X-*p* groups at higher temperatures may involve the formation of [$RhHCl(CO)_2$(RNNNR)] [(b) in Scheme 1], with equivalent *cis* carbonyls *cis* to the hydride ligand, by oxidative addition of the triazene to form a six-coordinate 18-electron triazenide hydride complex. The X-ray structural study of **2** supports this proposal, effectively showing the incipient formation of a Rh–H bond (Fig. 2). Moreover, just such an oxidative addition reaction occurs when [$RhH(PPh_3)_4$] reacts with PhNNNHPh to give the stable triazenide complex [$RhH_2(PPh_3)_2$(PhNNNPh)].[6]

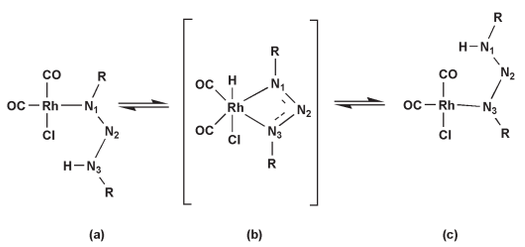

Scheme 1 R = aryl.

At −80 °C, the $^{13}C\{^{1}H\}$ NMR spectra (Table 8) of **1**–**4** also show inequivalent C_6H_4X-*p* groups. Moreover, in each case there are two doublets for the CO ligands, in the range δ 183.4–178.8 [$J(^{13}C^{103}Rh)$ 68–72 Hz], in agreement with the *cis*-$Rh(CO)_2$ unit

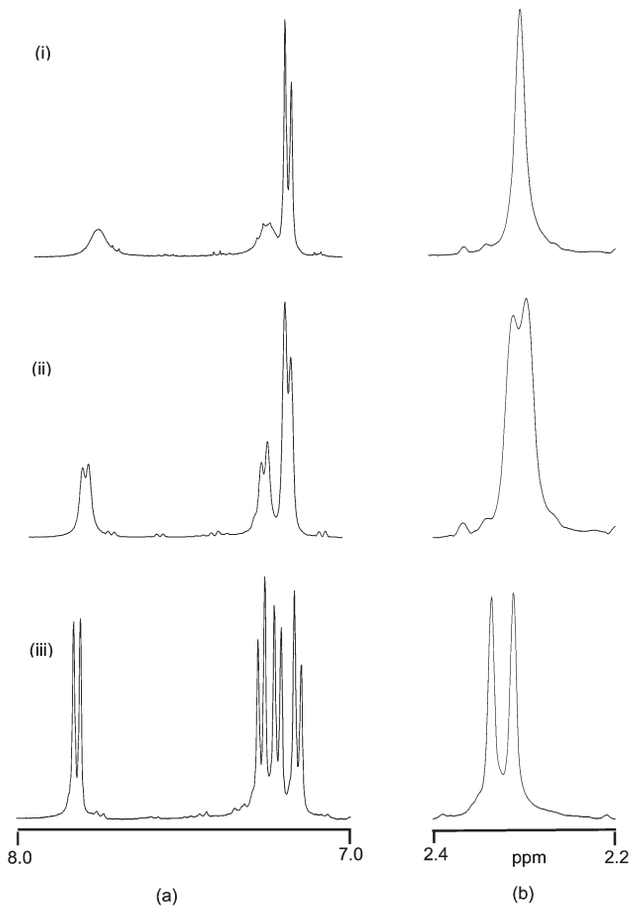

Fig. 7 ^{1}H NMR spectra of (a) the C_6H_4, and (b) the Me resonances of $[RhCl(CO)_2(p\text{-}MeC_6H_4NNNHC_6H_4Me\text{-}p)]$ **2**, at (i) 20 °C, (ii) −40 °C, (iii) −80 °C.

detected by IR spectroscopy and confirmed by X-ray crystallography.

Replacing the Rh atom of **2** with Ir gives **5**, the ^{1}H NMR spectrum of which is temperature invariant. Thus, between room temperature and −80 °C, two signals are observed for the methyl groups, at δ 2.34 and 2.32, and the NH proton is observed at δ 11.90. The reason for the different fluxional behaviour of **2** and **5** is not understood.

The ^{19}F NMR spectroscopic data for complex **4** at 20 and −80 °C are given in Table 9. The presence of two broad signals at 20 °C [Fig 8(i)] suggests that this is not the limiting high temperature spectrum. On lowering the temperature to −80 °C, each of these signals becomes a triplet of triplets due to coupling to the *ortho*- and *meta*-hydrogens of the $C_6H_4F\text{-}p$ groups [Fig. 8(ii)].

The fluxional process for $[PdCl(\eta^3\text{-}C_3H_5)(p\text{-}MeC_6H_4NNNHC_6H_4Me\text{-}p)]$ **6** can also be slowed sufficiently at −70 °C to observe inequivalent $C_6H_4Me\text{-}p$ groups and an asymmetric $\eta^3\text{-}C_3H_5$ group in the ^{1}H NMR spectrum (Table 10). At room temperature, there is one signal at δ 2.36 for the methyl protons and two doublets at δ 3.99 and 3.10 for the *syn* (H_a) and *anti* (H_b) protons of the allyl ligand. The multiplet centred at δ 5.48 corresponds to H_c [Fig. 9(i)]. This suggests the *syn* and *anti* protons are equivalent due to a fluxional process which also leads to equivalent $C_6H_4Me\text{-}p$ groups at room temperature. As for **2**, this may involve the formation, by oxidative addition, of $[PdHCl(\eta^3\text{-}C_3H_5)(p\text{-}MeC_6H_4NNNC_6H_4Me\text{-}p)]$, similar to the intermediate shown in Scheme 1, with chloride *trans* to the hydride ligand. On cooling the solution to −70 °C, the Me signal splits into two, at δ 2.32 and 2.29, and the signals for the allyl *syn* and *anti* protons split into four doublets at δ 3.24, 3.47, 3.85 and 4.07 [Fig 9(ii)]. Similarly, the $^{13}C\{^{1}H\}$ NMR spectrum at −80 °C (Table 11) shows two singlets, at δ 21.13 and 21.28, for the methyl carbon atoms and two, at δ 61.53 and 64.15 and 115.18 for the terminal allyl carbon atoms.

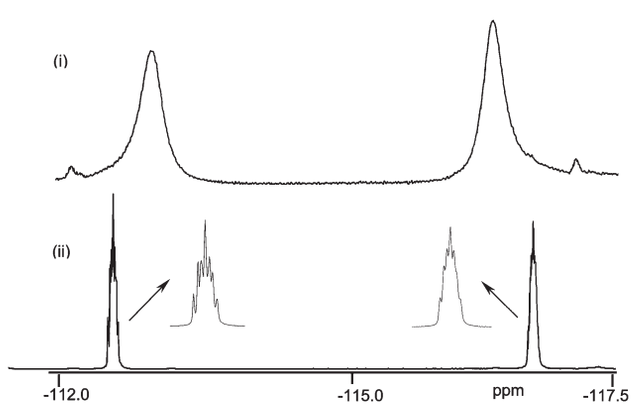

Fig. 8 ^{19}F NMR spectra of $[RhCl(CO)_2(p\text{-}FC_6H_4NNNHC_6H_4F\text{-}p)]$ **4**, at (i) 20 °C and (ii) −80 °C.

Table 8 $^{13}C\{^{1}H\}$ NMR spectroscopic data for $[MCl(CO)_2(RNNNHR)]$ in CD_2Cl_2 at −80 °C[a]

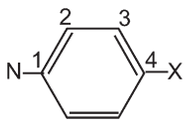

Complex	Chemical shift/ppm
1	183.28 [d, $J(^{13}C^{103}Rh)$ 68, CO], 178.96 [d, $J(^{13}C^{103}Rh)$ 72, CO], 148.09 (C^1), 138.33 (C^1), 129.95 (C^3), 129.42 (C^3), 128.87 (C^4), 126.06 (C^4), 122.09 (C^2), 116.47 (C^2)
2	183.32 [d, $J(^{13}C^{103}Rh)$ 68, CO], 179.04 [d, $J(^{13}C^{103}Rh)$ 72, CO], 145.83 (C^1), 139.10 (C^1), 135.98 (C^4), 135.95 (C^4), 130.42 (C^3), 129.87 (C^3), 121.74 (C^2), 116.21 (C^2), 21.33 (CH_3), 21.15 (CH_3)
3	183.16 [d, $J(^{13}C^{103}Rh)$ 68, CO], 178.88 [d, $J(^{13}C^{103}Rh)$ 72, CO], 146.25 (C^1), 145.34 (C^1), 142.41 (C^4), 136.23 (C^4), 129.31 (C^2), 128.77 (C^2), 121.80 (C^3), 116.32 (C^3), 28.66 (CH_2), 28.50 (CH_2), 15.95 (CH_3), 15.87 (CH_3)
4	183.31 [d, $J(^{13}C^{103}Rh)$ 68, CO], 178.89 [d, $J(^{13}C^{103}Rh)$ 72, CO], 163.79 (C^1), 161.82 (C^1), 160.50 (C^2), 158.57 (C^2), 144.41 (C^3), 134.73 (C^3), 123.79 [d, $J(^{13}C^{19}F)$ 9, C^4], 118.22 [d, $J(^{13}C^{19}F)$ 8, C^4]
5	171.55 (CO), 145.83 (C^1), 139.22 (C^1), 136.57 (C^4), 135.62 (C^4), 130.56 (C^3), 129.97 (C^3), 121.97 (C^2), 116.36 (C^2), 21.37 (CH_3), 21.24 (CH_3)

[a] J values in Hz.

Table 9 $^{19}F\{^{1}H\}$ spectroscopic data for $[RhCl(CO)_2(p\text{-}FC_6H_4NNNHC_6H_4F\text{-}p)]$ **4** in CD_2Cl_2[a]

Complex	T/°C	Chemical shift/ppm
4	20	−112.9, −116.2
	−80	−112.3, −116.8 [each tt, $J(^{19}F^{1}H)$ 5, 8]

[a] Chemical shifts (δ) in ppm.

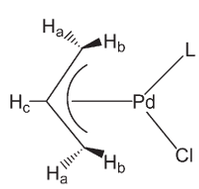

Experimental

The preparation, purification and reactions of the complexes described were carried out under an atmosphere of dry dinitrogen using dried, distilled and deoxygenated solvents; reactions were monitored by IR spectroscopy where necessary. The compounds $[\{Rh(\mu\text{-}Cl)(CO)_2\}_2]$,[7] $[\{M(\mu\text{-}Cl)Cl(PPh_3)\}_2]$ (M = Pd[8]

Table 10 ^{1}H NMR spectroscopic data for [PdCl(η^3-C_3H_5)(*p*-MeC_6H_4-$NNNHC_6H_4$Me-*p*)] **6** in CD_2Cl_2[a]

T/°C	Chemical shift/ppm
20	11.51 (s, 1H, NH), 7.46 (s br, 2H, C_6H_4), 7.20 (d, 6H, C_6H_4), 5.48 (m, 1H, allyl, H_c), 3.99 (d, 2H, $^3J_{HH}$ 6, allyl, H_a), 3.10 (d, 2H, $^3J_{HH}$ 13, allyl, H_b), 2.36 (s, 6H, CH_3)
−70	11.50 (s, 1H, NH), 7.46 (d, 2H, $^1J_{HH}$ 8, C_6H_4), 7.24 (d, 2H, $^1J_{HH}$ 8, C_6H_4), 7.07 (d, 2H, $^1J_{HH}$ 8, C_6H_4), 6.98 (d, 2H, $^1J_{HH}$ 8, C_6H_4), 5.62 (m, 1H, allyl, H_c), 4.07 (d, 1H, $^3J_{HH}$ 6, allyl, H_a), 3.85 (d, 1H, $^3J_{HH}$ 6, allyl, H_a), 3.47 (d, 1H, $^3J_{HH}$ 12, allyl, H_b), 3.24 (d, 1H, $^3J_{HH}$ 13, allyl, H_b), 2.32 (s, 3H, CH_3), 2.29 (s, 3H, CH_3)

[a] Chemical shifts (δ) in ppm, *J* values in Hz. Allyl numbering as below (L = *p*-$MeC_6H_4NNNHC_6H_4$Me-*p*).

Table 11 ^{13}C{^{1}H} NMR spectroscopic data for [PdCl(η^3-C_3H_5)(*p*-$MeC_6H_4NNNHC_6H_4$Me-*p*)] **6** in CD_2Cl_2 at −80 °C

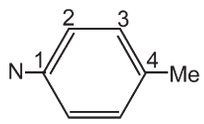

Complex	Chemical shift/ppm
6	147.45 (C^1), 137.92 (C^1), 137.61 (C^4), 134.27 (C^3), 129.96 (C^3), 129.38 (C^2), 122.07 (C^2), 116.53 (C^2), 115.18 (s, CH_2CHCH_2), 64.15 (s, CH_2CHCH_2), 61.53 (s, CH_2CHCH_2), 21.28 (CH_3), 21.13 (CH_3)

Table 12 Crystal and refinement data for **1**, **2**, **6** and **7**

Compound	**1**	**2**	**6**	**7**
Formula	$C_{14}H_{11}ClN_3O_2Rh$	$C_{16}H_{15}ClN_3O_2Rh$	$C_{17}H_{19}ClN_3Pd$	$C_{32}H_{29}Cl_2N_3PPt$
M	391.62	419.67	408.21	753.54
Crystal system	Monoclinic	Triclinic	Orthorhombic	Monoclinic
Space group (no.)	*C*2/*c* (15)	$P\bar{1}$ (2)	*Pbca* (61)	$P2_1$ (14)
a/Å	17.165(3)	9.202(3)	17.355(3)	11.404(2)
b/Å	10.403(2)	10.234(3)	9.906(2)	16.906(4)
c/Å	16.633(3)	10.509(3)	19.753(3)	15.680(3)
α/°	90	61.077(4)	90	90
β/°	96.922(3)	84.978(5)	90	90.428(13)
γ/°	90	79.941(5)	90	90
T/K	173(2)	173(2)	173(2)	193(2)
U/Å^3	2948.4(7)	852.9(4)	3395.9(10)	3020.2(10)
Z	8	2	8	4
μ/mm^{-1}	1.346	1.169	1.250	4.902
Reflections collected	9302	5468	22655	31862
Independent reflections (R_{int})	3394 (0.0341)	3770 (0.0195)	3897 (0.0713)	13667 (0.0585)
Final *R* indices [$I > 2\sigma(I)$]: R_1, wR_2	0.0302, 0.0660	0.0311, 0.0668	0.0487, 0.1022	0.0322, 0.0664

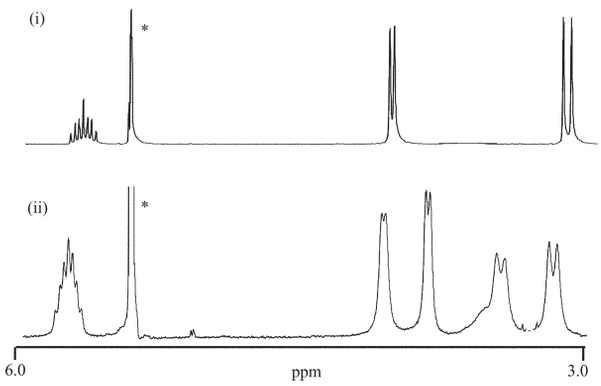

Fig. 9 ^{1}H NMR spectra of the η^3-C_3H_5 resonances of [PdCl(η^3-C_3H_5)(*p*-$MeC_6H_4NNNHC_6H_4$Me-*p*)] **6**, at (i) 20 °C, (ii) −70 °C. The peak marked with an asterisk, *, is due to CD_2Cl_2.

or Pt[9]), [{Pd(μ-Cl)(η^3-C_3H_5)}$_2$],[10] and *p*-$XC_6H_4NNNHC_6H_4X$-*p* (X = H, Me, Et and F)[11] were prepared by published methods. New complexes were purified using a mixture of two solvents. The impure solid was dissolved in the more polar solvent, the resulting solution was filtered and then treated with the second solvent, and the mixture reduced in volume *in vacuo* to induce precipitation. IR spectra were recorded on a Nicolet 5ZDX FT spectrometer. ^{1}H NMR spectra were recorded on a Jeol GX270, GX 400 or λ300 spectrometers with $SiMe_4$ as an internal standard. ^{19}F, ^{31}P and ^{13}C NMR spectra were recorded on a Jeol λ300 spectrometer. Microanalyses were carried out by the staff of the Microanalytical Service of the School of Chemistry, University of Bristol.

Syntheses

[RhCl(CO)$_2$(*p*-$MeC_6H_4NNNHC_6H_4$Me-*p*)] 2. To a stirred solution of [{Rh(μ-Cl)(CO)$_2$}$_2$] (0.104 g, 0.268 mmol) in CH_2Cl_2 (20 cm^3) was added *p*-$MeC_6H_4NNNHC_6H_4$Me-*p* (0.12 g, 0.536 mmol). After 10 min the yellow solution was filtered through Celite and the solvent evaporated to low volume (*ca.* 5 cm^3) *in vacuo*. *n*-Hexane (10 cm^3) was added to precipitate a yellow powder which was washed with *n*-hexane (2 × 20 cm^3) and dried *in vacuo*, yield 182 mg (81%).

The complexes [RhCl(CO)$_2$(*p*-$XC_6H_4NNNHC_6H_4$X-*p*)] (X = H **1**, Et **3**, F **4**) were prepared similarly.

The complexes [PdCl(η^3-C_3H_5)(*p*-$MeC_6H_4NNNHC_6H_4$Me-*p*)] **6**, *trans*-[$PtCl_2(PPh_3)$(*p*-$MeC_6H_4NNNHC_6H_4$Me-*p*)] **7** and *cis*- and *trans*-[$PdCl_2(PPh_3)$(*p*-$MeC_6H_4NNNHC_6H_4$Me-*p*)] **8** were prepared similarly as yellow powders, on replacing [{Rh(μ-Cl)(CO)$_2$}$_2$] by [{Pd(μ-Cl)(η^3-C_3H_5)}$_2$] [{Pt(μ-Cl)Cl(PPh_3)}$_2$] and [{Pd(μ-Cl)Cl(PPh_3)}$_2$], respectively.

Structure determinations of [RhCl(CO)$_2$(PhNNNHPh)] 1, [RhCl(CO)$_2$(*p*-$MeC_6H_4NNNHC_6H_4$Me-*p*)] 2, [PdCl(η^3-C_3H_5)(*p*-$MeC_6H_4NNNHC_6H_4$Me-*p*)] 6, and *trans*-[$PtCl_2(PPh_3)$(*p*-$MeC_6H_4NNNHC_6H_4$Me-*p*)] 7

Many of the details of the structure analyses of **1**, **2**, **6** and **7** are listed in Table 12. All structure analyses were carried out by standard low-temperature area detector methods.

CCDC reference numbers 240474–240477.

See http://www.rsc.org/suppdata/dt/b4/b408410a/ for crystallographic data in CIF or other electronic format.

Acknowledgements

We thank the University of Bristol and the EPSRC for Postgraduate Scholarships (to K. M. A. and R. A. B., respectively).

References

1 See, for example: N. G. Connelly, G. Garcia, M. Gilbert and J. S. Stirling, *J. Chem. Soc., Dalton Trans.*, 1987, 1403; D. C. Boyd, N. G. Connelly, G. Garcia Herbosa, M. G. Hill, K. R. Mann,

C. Mealli, A. G. Orpen, K. E. Richardson and P. H. Rieger, *Inorg. Chem.*, 1994, **33**, 960; N. G. Connelly, P. R. G. Davis, E. E. Harry, P. Klangsinsirikul and M. Venter, *J. Chem. Soc., Dalton Trans.*, 2000, 2273.
2 N. G. Connelly and G. Garcia, *J. Chem. Soc., Dalton Trans.*, 1987, 2737.
3 N. G. Connelly, O. D. Hayward, P. Klangsinsirikul, A. G. Orpen and P. H. Rieger, *Chem. Commun.*, 2000, 963.
4 V. F. Gladkova and Y. D. Kondrashev, *Kristallografiya*, 1972, **17**, 33, (*Chem. Abstr.*, 1972, **76**, 132697m).
5 G. Bombieri, A. Immirzi and L. Toniolo, *Transition Met. Chem.*, 1976, **1**, 130.
6 K. R. Laing, S. D. Robinson and M. F. Uttley, *J. Chem. Soc., Dalton Trans.*, 1974, 1205.
7 J. A. McCleverty and G. Wilkinson, *Inorg. Synth.*, 1990, **28**, 84.
8 R. Uson, J. Fornies and F. Martinez, *J. Organomet. Chem.*, 1977, **132**, 429.
9 A. C. Smithies, P. Schmidt and M. Orchin, *Inorg. Synth.*, 1970, **12**, 240.
10 Y. Tatsuno, T. Yoshida and S. Otsuka, *Inorg. Synth.*, 1979, **19**, 220.
11 W. W. Hartman and J. B. Dickey, *Org. Synth.*, 1943, Collect. Vol. II, 163.